First Structural Characterization of Binary As^{III} and Sb^{III} Azides

Ralf Haiges,*[a] Ashwani Vij,*[b] Jerry A. Boatz,[b] Stefan Schneider,[a] Thorsten Schroer,[a] Michael Gerken,[a] and Karl O. Christe*[a, b]

Abstract: The highly explosive molecules $As(N_3)_3$ and $Sb(N_3)_3$ were obtained in pure form by the reactions of the corresponding fluorides with $(CH_3)_3SiN_3$ in SO_2 and purification by sublimation. The crystal structures and ^{14}N NMR, infrared, and Raman spectra were determined, and the results compared to ab initio second-order perturbation theory calculations. Whereas $Sb(N_3)_3$ possesses a propeller-shaped, pyramidal structure with perfect C_3 symmetry, the $As(N_3)_3$ molecule is significantly distorted from C_3 symmetry due to crystal packing effects.

Keywords: ab initio calculations · antimony · arsenic · azides · structure elucidation · vibrational spectroscopy

Introduction

The syntheses of the highly explosive binary triazides of arsenic and antimony have recently been reported.[1–4] However, the structures of these interesting compounds could not be determined because they were difficult to crystallize or obtained only as oils. We have now been able to prepare $M(N_3)_3$ (M = As, Sb) as very pure solids and obtained their single crystals by slow and careful sublimation of the solids.

Results and Discussion

Syntheses and properties: The reaction of AsF_3 or SbF_3 in SO_2 with excess $(CH_3)_3SiN_3$ at room temperature results in complete azide–fluoride exchange yielding a clear solution of $As(N_3)_3$ or precipitation of $Sb(N_3)_3$, respectively, according to Equation (1) (M = As, Sb).

$$MF_3 + 3\,(CH_3)_3SiN_3 \xrightarrow{SO_2} M(N_3)_3 + 3\,(CH_3)_3SiF \qquad (1)$$

Removal of the volatile compounds, SO_2, $(CH_3)_3SiF$, and excess $(CH_3)_3SiN_3$, at ambient temperature results in pure triazides.

$As(N_3)_3$, which had previously been prepared by the reaction of $AsCl_3$ with NaN_3 and been reported to be a yellowish liquid,[1] was obtained as a white solid. Single crystals of arsenic triazide were obtained by slow and careful sublimation in a dynamic vacuum. The crystalline product melts at 37 °C. The molten $As(N_3)_3$ decomposes at 62 °C, resulting in a milky liquid that explodes at about 160 °C.

Crude $Sb(N_3)_3$ was isolated as a white solid with a decomposition point of 130 °C. Despite previous reports of explosive decomposition upon attempted sublimation,[2] we were able to obtain colorless crystals by sublimation of the crude product in a static vacuum at 100–110 °C. It should be emphasized that $As(N_3)_3$ and $Sb(N_3)_3$ are sensitive to mechanical shock and can explode violently.

Crystal structure of $As(N_3)_3$: Clear colorless $As(N_3)_3$ crystallizes in the monoclinic system (Table 1). The crystal structure of $As(N_3)_3$ is shown in Figure 1, and the atomic coordinates and bond lengths are listed in Tables 2 and 3. The three azido groups are arranged in a pyramidal, propeller-type fashion, which is in contrast to the $[C(N_3)_3]^+$ ion, which exhibits a trigonal planar arrangement for the central carbon atom and the three α-nitrogen atoms.[5] This difference in the structures of $M(N_3)_3$ (M = As, Sb) and $[C(N_3)_3]^+$ is due to the presence of a sterically active lone valence electron pair on As and Sb (see Figure 2).

The presence of a sterically active, free valence-electron pair on As was verified both experimentally and theoretically. Experimentally, a difference electron-density contouring of the X-ray diffraction data clearly shows the presence of the free pair (see Figure 3a). Theoretically, the RHF/6–

[a] Dr. R. Haiges, Dr. S. Schneider, Dr. T. Schroer, Dr. M. Gerken, Prof. K. O. Christe
Loker Research Institute
University of Southern California
Los Angeles, CA 90089–1661 (USA)
Fax: (+1) 213-740-6679
E-mail: kchriste@usc.edu

[b] Dr. A. Vij, Dr. J. A. Boatz, Prof. K. O. Christe
ERC, Inc. and Space and Missile Propulsion Division
Air Force Research Laboratory (AFRL/PRSP)
10 East Saturn Boulevard, Bldg 8451
Edwards Air Force Base, CA 93524 (USA)
E-mail: kchriste@usc.edu

DOI: 10.1002/chem.200305482

Table 1. Crystal data and structure refinement for $As(N_3)_3$ and $Sb(N_3)_3$.

	$As(N_3)_3$	$Sb(N_3)_3$
formula	AsN9	N9Sb
M_r	201.01	247.84
T [K]	213(2)	223(2)
space group	$P2_1/c$	$R\bar{3}$
a [Å]	7.3263(7)	7.6998(9)
b [Å]	11.716(1)	
c [Å]	6.9865(7)	
α [°]	90	55.79(2)
β [°]	107.219(2)	
V [Å^3]	572.8(1)	291.26(6)
Z	4	2
ρ_{calcd} [g cm^{-3}]	2.331	2.826
μ [mm^{-1}]	5.863	4.667
crystal size [mm]	$0.34\times0.25\times0.14$	$0.12\times0.10\times0.08$
λ [Å]	0.71073	0.71073
R_{int}	0.0272	0.0422
transmission factors	0.4941, 0.2404	0.7065, 0.6043
goodness-of-fit on F	1.098	1.132
$R1$, $wR2$ $[I>2\sigma(I)]$	0.0240 0.0641	0.0320, 0.0849
$R1$, $wR2$ (all data)	0.0254, 0.0650	0.0328, 0.0856

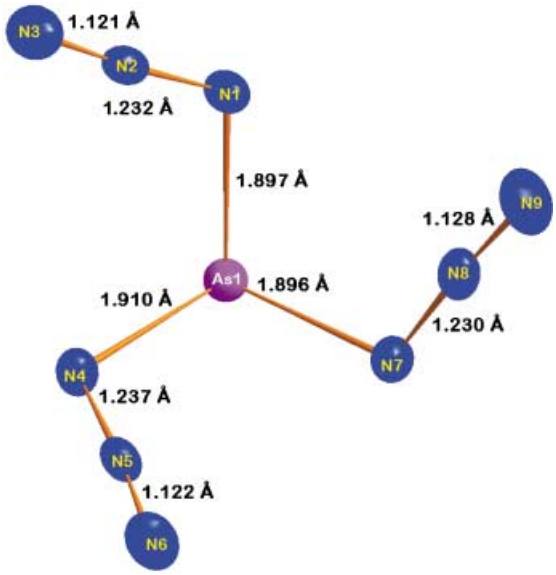

Figure 1. An ORTEP plot of $As(N_3)_3$ with displacement ellipsoids at the 40% probability level.

Table 2. Atomic coordinates ($\times10^4$) and equivalent isotropic displacement parameters [Å$^2\times10^3$] for $As(N_3)_3$. U_{eq} is defined as one third of the trace of the orthogonalized U_{ij} tensor.

	x	y	z	U_{eq}
As1	2858(1)	4451(1)	6183(1)	21(1)
N1	1116(3)	4819(2)	3655(3)	27(1)
N2	1725(3)	4783(2)	2190(3)	22(1)
N3	2190(3)	4790(2)	799(3)	35(1)
N4	4850(3)	3837(2)	5241(3)	25(1)
N5	4994(2)	2785(2)	5223(3)	23(1)
N6	5226(3)	1840(2)	5180(4)	37(1)
N7	1743(3)	3030(2)	6499(3)	26(1)
N8	250(3)	2776(2)	5209(3)	27(1)
N9	-1129(3)	2495(2)	4091(4)	41(1)

Table 3. Bond lengths [Å], bond angles [°], and torsion angles for $As(N_3)_3$ and $Sb(N_3)_3$.

	$As(N_3)_3$	$Sb(N_3)_3$
M–N1	1.897(2)	2.119(4)
M–N4	1.910(2)	2.119(4)[a]
M–N7	1.896(2)	2.119(4)[b]
N1–N2	1.232(3)	1.233(6)
N2–N3	1.121(3)	1.131(6)
N4–N5	1.237(3)	1.233(6)[a]
N5–N6	1.122(3)	1.131(6)[a]
N7–N8	1.231(3)	1.233(6)[b]
N8–N9	1.128(3)	1.131(6)[b]
N1-M-N4	97.87(9)	90.1(2)
N1-M-N7	96.51(9)	90.1(2)[a]
N7-M-N4	96.22(8)	90.1(2)[b]
N2-N1-M	117.1(2)	115.8(3)
N5-N4-M	117.1(2)	115.8(3)[a]
N8-N7-M	116.6(2)	115.8(3)[b]
N3-N2-N1	175.9(2)	178.3(5)
N6-N5-N4	175.8(2)	178.3(5)[a]
N9-N8-N7	176.3(2)	178.3(5)[b]
M-N1-N2-N3	161(4)	148(17)
M-N4-N5-N6	171(4)	
M-N7-N8-N9	171(4)	
N1-M-N4-N5	102.5(2)	
N1-M-N7-N8	5.1(2)	
N4-M-N1-N2	11.9(2)	9.9(3)
N4-M-N7-N8	103.8(2)	
N7-M-N1-N2	109.1(2)	100.1(3)
N7-M-N4-N5	5.0(2)	

[a] Transformation = z, x, y. [b] Transformation = y, z, x.

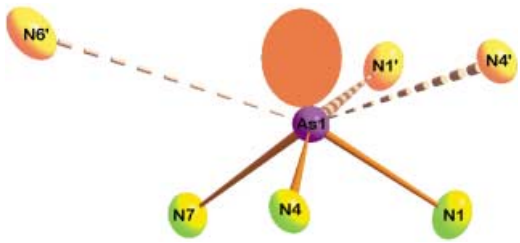

Figure 2. An ORTEP plot of $As(N_3)_3$ at the 40% probability level showing the sterically active free valence-electron pair of arsenic and the three closest nitrogen contacts that give the arsenic atom a coordination number of seven.

31G(d) Boys localized orbitals[6] of the C_3(anti) local minimum geometry were computed, and a two-dimensional contour plot of the sterically active lone pair on the arsenic atom is shown in Figure 3b. Similarly, the MP2/6–31G(d) total electron density was analyzed by using Bader's Atoms in Molecules (AIM) method.[7] A two-dimensional contour plot of the laplacian of the total electron density (i.e., $\nabla^2\rho$) is shown in Figure 3c. The localized negative region of the laplacian on the arsenic atom along the direction of the C_3 symmetry axis is consistent with the presence of a sterically active lone pair.

In $As(N_3)_3$, the three azido groups point away from the arsenic lone pair. The torsion angles (Table 3) clearly show that the $As(N_3)_3$ structure lacks perfect C_3 symmetry. The values for the N7-As1-N4-N5 and N1-As1-N7-N8 angles are similar with 5.0(2) and 5.1(2)°, respectively, but different

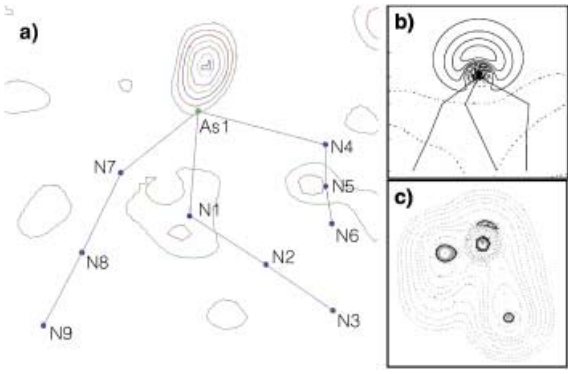

Figure 3. Experimental and theoretical evidence for the presence of a sterically active free valence-electron pair in $As(N_3)_3$: a) Difference electron density contour from the X-ray diffraction data. b) Contour plot of the RHF/6–31G(d) Boys localized sterically active lone pair orbital on As, in a plane containing the C_3 symmetry axis of the C_3(*anti*) structure; solid and dashed contours correspond to positive and negative values, respectively; the spacing between contour lines is 0.05 $bohr^{3/2}$. c) Contour plot of the MP2/6–31G(d) laplacian of the total electron density of the C_3(*anti*) geometry, in a plane containing the C_3 symmetry axis; solid and dashed lines correspond to negative and positive values, respectively.

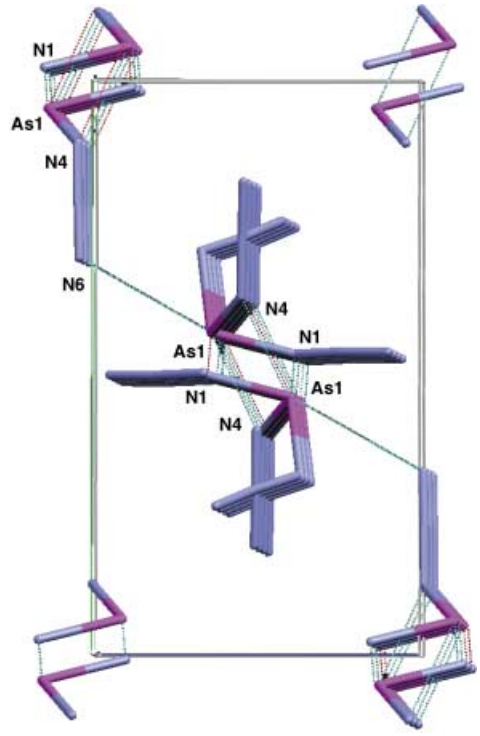

Figure 5. Crystal packing of $As(N_3)_3$, viewed along the chains and the *a* axis, showing the stacking of the arsenic–nitrogen parallelograms around the inversion centers along the origin and cell edges. The individual chains are linked to each other through diagonal As1–N6 contacts that penetrate the *ab* plane.

from the N4-As1-N1-N2 angle of 11.9(2)°, indicating the presence of nonequivalent azido groups. A mean least-squares planes analysis of the azido groups relative to the plane formed by the three α-nitrogen atoms further substantiates the nonequivalence of these groups. The twists of the azido groups N1-N2-N3, N4-N5-N6, and N7-N8-N9 relative to the mean plane formed by N1, N4, and N7 are 46.9(2), 43.0(2) and 57.9(3)°, respectively.

Packing diagrams for $As(N_3)_3$ are shown in Figures 4 and 5. It is well known that arsenic atoms can accommodate at least six closely packed fluoride ligands, as in AsF_6^-. It is, therefore, not surprising that arsenic seeks a coordination number higher than four in $As(N_3)_3$. For $SbCl(N_3)_2$, it has previously been shown[8] that the antimony atom can expand its coordination number by the formation of nitrogen bridges involving the α-nitrogen atoms of the azido ligands. This bridging mode results in four-membered rings containing two antimony and two N_α atoms. These rings are interconnected through the antimony atoms, thus forming infinite zigzag chains. The same bridging principle is observed for $As(N_3)_3$, in which two of its azido groups, N1-N2-N3 and N4-N5-N6, participate in the formation of the infinite chain structure through the formation of fused As_2N1_2 and As_2N4_2 dimeric parallelograms (see Figure 4). These chains run along the *a* axis with the two parallelograms twisted at ~74° with respect to each other. The bridge bond lengths are 2.970 Å for the rings involving the N4 atoms and 3.069 Å for the rings involving the N1 atoms. The nonequivalence of the two rings is caused by N6 forming an additional bridge of 3.198 Å to an arsenic atom of a neighboring chain, perpendicular to the *ab* plane, thus interconnecting the

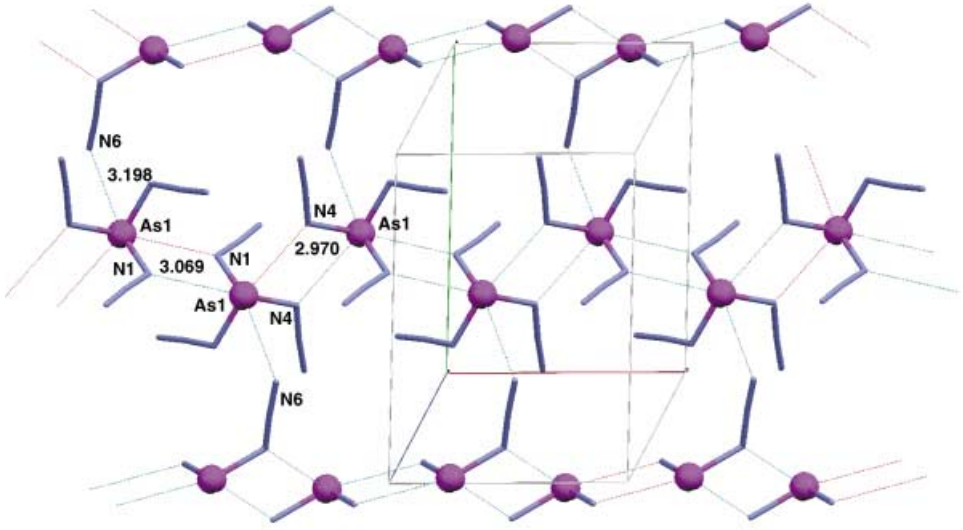

Figure 4. Crystal packing of $As(N_3)_3$ along the *b* axis showing the zig-zag arrangement of alternating $As1_2N1_2$ and $As1_2N4_2$ parallelograms. These chains run along the *a* axis and are linked to adjacent chains by As1–N6 bonds. The N7-N8-N9 azido groups do not participate in the bridging.

individual chains to form a three dimensional network (see Figure 5). Like the chlorine ligand in $SbCl(N_3)_2$, the third azido ligand, N7-N8-N9, does not participate in the bridging. This packing arrangement accounts for the nonequivalence of the three azido ligands in $As(N_3)_3$ and provides the arsenic atoms with a coordination number of seven with three azido ligands, three nitrogen bridges, and one free valence-electron pair. The arrangement is that of a distorted monocapped octahedron, with the free valence-electron pair occupying the monocap position. The angle, formed by the bridge bonds, is significantly larger than that between the azido ligands (Figure 2). The relative ease with which crystal packing effects can deform the $As(N_3)_3$ structure from the ideal C_3 symmetry is also supported by the theoretical calculations (see below). It was found that the four stable isomers, which exhibit different orientations of the azido groups, differ in energy by a mere 3 kcal mol^{-1} or less.

Crystal structure of of $Sb(N_3)_3$: This molecule (Figure 6 and Tables 3 and 4) represents a "text-book" example of perfect C_3 symmetry. The asymmetric SbN_3 unit has an azido group

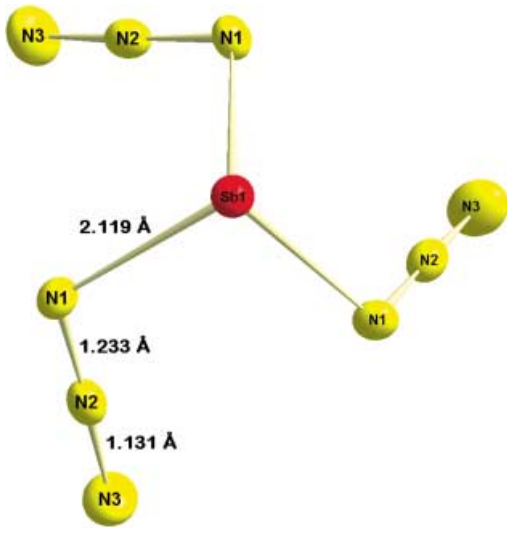

Figure 6. An ORTEP plot of $Sb(N_3)_3$ with displacement ellipsoids at the 40% probability level.

Table 4. Atomic coordinates ($\times 10^4$) and equivalent isotropic displacement parameters [Å$^2 \times 10^3$] for $Sb(N_3)_3$. U_{eq} is defined as one third of the trace of the orthogonalized U_{ij} tensor.

	x	y	z	U_{eq}
Sb1	6897(1)	6897(1)	6897(1)	21(1)
N1	8642(6)	6330(6)	3834(7)	22(1)
N2	7558(7)	7362(7)	2605(7)	24(1)
N3	6612(8)	8311(8)	1432(8)	39(1)

covalently bonded to the antimony atom that lies on a threefold rotational axis. The symmetry operations z,x,y and y,z,x for a rhombohedral setting for space group $R\bar{3}$ generate the remaining two azido groups, thus placing the antimony atom at the pivot of a propeller-shaped molecule. The Sb–N distance of 2.119(4) Å is shorter than the two Sb–N distances of 2.152(8) and 2.1444(7) Å found in the crystal structure of $SbCl(N_3)_2$.[8] The azido groups are almost linear with N-N-N angles of 178.3(5)°. As found for the $As(N_3)_3$ structure, the N_α–N_β distance of 1.233(6) Å is longer than the N_β–N_γ distance of 1.131(6) Å. However, in the case of $SbCl(N_3)_2$,[8] one of the azido groups has an "abnormal" N_α–N_β distance of 0.98(1) Å, which is shorter than the N_β–N_γ distance of 1.28(1) Å. This peculiarity has also been observed by us for mixed chloride/azide antimony(v) anions, $[Ph_4M]^+[SbCl_x(N_3)_{6-x}]^-$ ($x=2$–5; M = P or As) and the $Te(N_3)_5^-$ ion,[9] and by others for the structures of some azido derivatives of platinum,[10–12] vanadium,[13] and tantalum.[14] In our opinion, these unusually short distances are not real and are due to partial occupancy of some azide sites by other atoms, such as chlorine.

In $Sb(N_3)_3$ and $SbCl(N_3)_2$, the angles at the Sb atom are compressed from an ideal tetrahedral value of 109.5° to ~90°. This angle compression is caused by the increased repulsion from the sterically active free valence-electron pair on antimony. Because this effect increases with increasing size of the central atom, it is less pronounced for $As(N_3)_3$, which exhibits an N-As-N angle of 97.9°, and for isoelectronic $Te(N_3)_3^+$ in its SbF_6^- salt. The latter is significantly distorted from ideal C_3 symmetry due to crystal packing effects and fluorine bridging, and exhibits N-Te-N angles ranging from 91.9° to 97.3°.[15] Furthermore, the Sb-N-N angles of 115.8(3)° in $Sb(N_3)_3$ are smaller than those of ~120° found in $SbCl(N_3)_2$.[8] In accord with the requirements for C_3 symmetry, the torsion angles in $Sb(N_3)_3$ are all identical and, due to the almost linear azide group (178.3(5)°), the M-N-N-N torsion angles are poorly determined.

One of the most interesting consequences of the high symmetry of $Sb(N_3)_3$ is its crystal packing. Figure 7 shows aesthetically pleasing views down the z (111) axis. Each of the molecules has a threefold local symmetry, but the z axis also constitutes the crystallographic threefold axis. When no bonds are displayed, the nitrogen packing mimics the "Star of David". However, when all bonds are displayed, an inorganic pseudo[18]crown-6 evolves in which six antimony atoms form a perfect hexagon and encapsulate two $Sb(N_3)_3$ molecules located on a pseudo-S_6 axis passing through the center of the hexagonal cell. The two central $Sb(N_3)_3$ molecules are stacked with the lone pairs on antimony pointing away from each other and the three azido groups on each antimony being rotated by 60° from each other, forming a perfectly staggered structure. When viewed from the top, each individual $Sb(N_3)_3$ unit resembles the three legged "Isle of Man" emblem.

When viewed from the side (see Figure 8), the packing can be described as a sheet structure. Within each sheet, there are two $Sb(N_3)_3$ layers. The antimony atoms of each layer point in opposite directions and form triangular funnel-like holes. The antimony atoms of one layer are located deep inside the holes of the other layer and reside ~0.9 Å beyond the plane formed by the antimony atoms of the other layer. The resulting close contact between the two layers allows each antimony to form three close contacts of 2.844 Å with α-nitrogen atoms from three neighboring $Sb(N_3)_3$ units, thus creating two-dimensional sheets (see

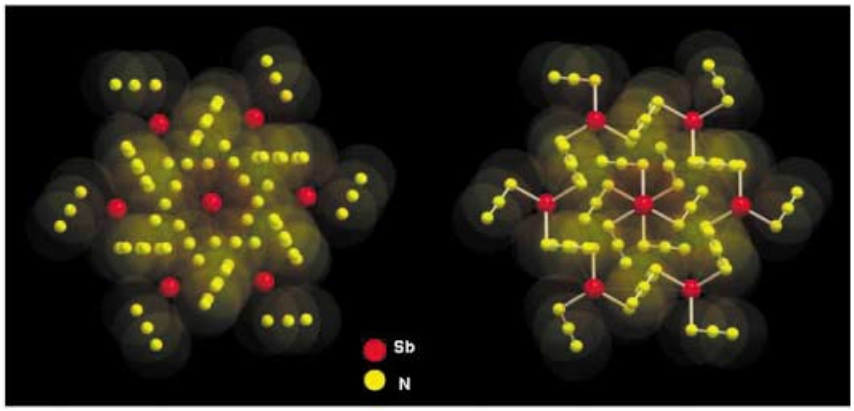

Figure 7. Packing diagrams of $Sb(N_3)_3$ viewed again along the z axis. The left-hand picture, in which the nitrogen atoms are highlighted in yellow forms a "Star of David" pattern, while in the right-hand picture, the addition of the connecting bonds emphasizes the six-fold high symmetry of the structure and gives the appearance of a crown made up from "Isle of Man" emblem subunits.

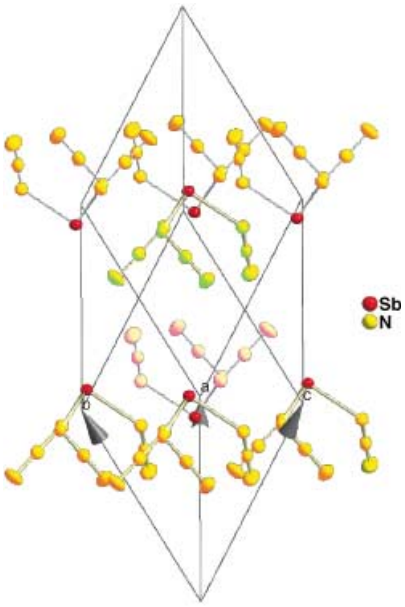

Figure 8. Side view of the $Sb(N_3)_3$ structure showing two sheets interconnected through staggered azido groups.

Figure 9). This gives antimony a total coordination number of seven (three equivalent azido ligands, three equivalent nitrogen bridges, and one sterically active, free valence-electron pair). Because of the increased repulsion from the free valence-electron pair of antimony, the angle between the Sb···N bridges is opened to 118.7°, while the N-Sb-N angle is compressed to about 90°. The Sb···N bridges result in the formation of three α-nitrogen-bridged, perfectly planar, four-membered rings around each antimony atom. A mean least-square plane analysis shows that they form angles of 76.6° with each other and are arranged in a fashion resembling the "Mitsubishi" emblem (see insert in Figure 9). The contacts between the sheets consist of staggered azido groups that are rotated by 60°with respect to each other.

The $Sb(N_3)_3$ and $As(N_3)_3$ packings have several features in common. In both structures, the central atoms have coordination numbers of seven with three azide ligands, three nitrogen bridges, and one sterically active free valence-electron pair. Furthermore, both molecules associate through the formation of N_α-bridged four-membered rings. However, in $Sb(N_3)_3$, all three N_α atoms participate equally in the bridge formation (see "Mitsubishi" insert in Figure 9), while in $As(N_3)_3$ only two N_α atoms and one N_γ atom are involved ("half-Mitsubishi", see Figure 10). This results in a ribbon-like structure for $As(N_3)_3$ and a sheet structure for $Sb(N_3)_3$. Also, the bridges in $Sb(N_3)_3$ are much stronger

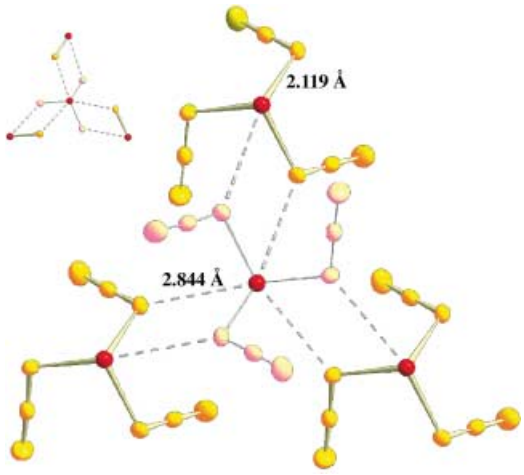

Figure 9. Nitrogen bridging within the $Sb(N_3)_3$ sheets. The insert shows the "Mitsubishi emblem" pattern of the bridging.

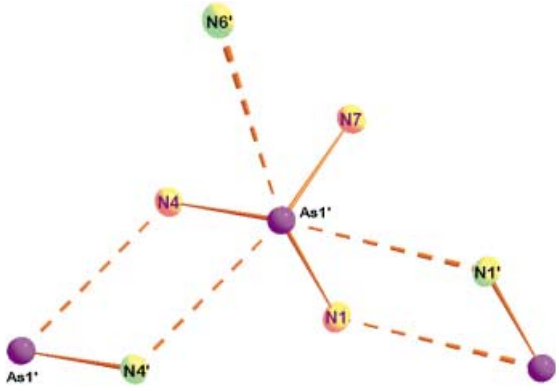

Figure 10. Nitrogen bridging within the $As(N_3)_3$ chains, showing a "Half-Mitsubishi" pattern.

(2.844 Å, while the sum of the covalent van der Waals radii is 3.66 Å) than those in $As(N_3)_3$ (2.970, 3.069, and 3.198 Å, while the sum of the covalent van der Waals radii is only 3.40 Å).

^{14}N NMR spectra: As expected for covalently bonded azides,[4] three well-resolved resonances were found for both compounds in their ^{14}N NMR spectra in CH_2Cl_2 at 25 °C. The $As(N_3)_3$ molecule shows a very broad signal at $\delta = -290$ ppm ($\Delta\nu_{1/2} = 300$ Hz) for the N_α atoms, a sharp signal at $\delta = -145.3$ ppm ($\Delta\nu_{1/2} = 14$ Hz) for the N_β atoms, and a medium-sharp resonance at $\delta = -175.9$ ppm ($\Delta\nu_{1/2} = 34$ Hz) for the N_γ atoms. This is in disagreement with the data previously reported for this compound, $\delta = -318.0$ (N_α), -131.1 (N_β), and -165.2 ppm (N_γ).[1,16] However, the observed ^{14}N NMR resonances for $Sb(N_3)_3$ of $\delta = -324.5$ ($\Delta\nu_{1/2} = 139$ Hz, N_α), -136.2 ($\Delta\nu_{1/2} = 18$ Hz, N_β), and -172.3 ppm ($\Delta\tilde{\nu}_{1/2} = 23$ Hz, N_γ) are in good agreement with the data reported previously.[2]

Theoretical calculations: Geometry optimizations were performed for $As(N_3)_3$ and $Sb(N_3)_3$ by using second-order perturbation theory methods (MP2, also known as MBPT(2)).[17,18] All stationary points were verified as local minima through diagonalization of the matrix of energy second derivatives with respect to nuclear displacements (i.e., the hessian matrix).

Four local minima were located for $As(N_3)_3$ (see Figure 11 and Table 5). Zero-point vibrational-energy corrections for these minima differed by less than 0.1 kcal mol^{-1}. In the most stable minimum at the MP2 level, (**3**, C_1), two azido ligands adopt an approximate *anti*-orientation relative to the stereochemically active lone pair on the As atom, with the remaining azido ligand in a *gauche*-like orientation. The second most stable isomer (**1**, C_3) is 0.4 kcal mol^{-1} higher in energy than **3** and has all three azido ligands in an *anti* orientation. The isomer with two *gauche* azido ligands and one *anti* azido ligand (**2**) has C_s symmetry and is 0.7 kcal mol^{-1} higher in energy than **3**. Finally, the least stable minimum (**4**) has all three azido groups in a *gauche* orientation (C_3 symmetry) and is 3.0 kcal mol^{-1} higher in energy than **3**. The observed crystal structure is best described as a somewhat distorted C_3 structure with the three azido ligands in an *anti* configuration. The calculated small energy differences can account for the ease with which this compound can distort from the ideal C_3 symmetry under the influence of crystal packing effects.

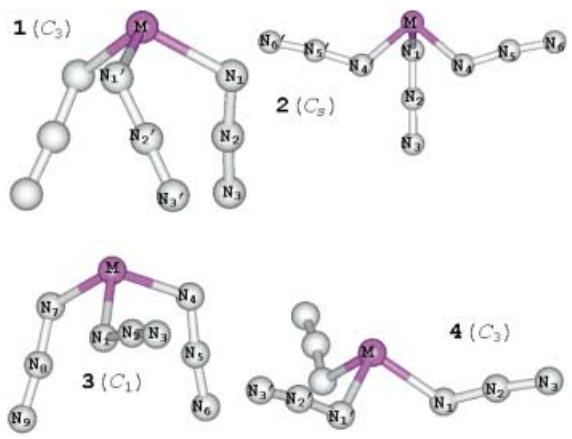

Figure 11. Local minima calculated for $As(N_3)_3$ (**1**–**4**) and $Sb(N_3)_3$ (**1** and **3**) at the MP2 level of theory. The values for the calculated bond lengths, bond angles, and torsion angles are given in Table 5.

Table 5. Calculated bond lengths [Å], bond angles [°], and torsion angles [°] for the local minima (**1**–**4**; see Figure 11) $As(N_3)_3$ (the values for $Sb(N_3)_3$ for minima **1** and **3** are given in parantheses) at the MP2 level of theory.

Compound **1**: $E = +0.4$ kcal mol^{-1} (0.0)			
M–N1	1.888 (2.069)	N2–N3	1.171 (1.196)
N1–N2	1.245 (1.267)		
N1-M-N1′	99.4 (96.2)	N3-N2-N1	175.0 (174.5)
N2-N1-M	117.6 (115.1)		
N3-N2-N1-M	164.9 (160.6)	N2-N1-M-N1′	81.7 (19.5)
Compound **2**: $E = +0.7$ kcal mol^{-1}			
M–N1	1.876	M–N4	1.877
N1–N2	1.246	N4–N5	1.246
N2–N3	1.170	N5–N6	1.171
N1-M-N4	99.9	N5-N4-M	117.9
N4-M-N4′	87.1	N3-N2-N1	174.6
N2-N1-M	117.2	N6-N5-N4	172.6
N3-N2-N1-M	180.0	N5-N4-M-N1	89.8
N6-N5-N4-M	180.0	N5-N4-M-N4	170.7
N2-N1-M-N4′	44.4		
Compound **3**: $E = 0.0$ kcal mol^{-1} (0.6)			
M–N1	1.893 (2.065)	N7–N6	1.246 (1.268)
M–N4	1.883 (2.063)	N2–N3	1.172 (1.199)
M–N7	1.865 (2.046)	N5–N6	1.171 (1.197)
N1–N2	1.243 (1.262)	N8–N9	1.169 (1.194)
N4–N5	1.245 (1.267)		
N1-M-N4	98.7 (95.3)	N8-N7-M	118.8 (117.2)
N4-M-N7	101.9 (98.2)	N3-N2-N1	173.6 (174.2)
N1-M-N7	92.5 (89.2)	N6-N5-N4	174.7 (174.7)
N2-N1-M	118.7 (120.5)	N9-N8-N7	173.6 (173.2)
N5-N4-M	118.0 (114.5)		
Compound **4**: $E = +3.0$ kcal mol^{-1}			
M–N1	1.871	N2–N3	1.171
N1–N2	1.245		
N1-M-N1′	93.4	N3-N2-N1	172.8
N2-N1-M	118.0		
N3-N2-N1-M	178.2	N2-N1-M-N1′	102.3

For $Sb(N_3)_3$, two local minima with C_3 and C_1 symmetry were located, with virtually identical zero-point vibrational-energy corrections. The C_3 structure has all azido ligands oriented *anti* with respect to the Sb lone pair. In the C_1 minimum, which is 0.6 kcal mol^{-1} less stable than the C_3 isomer, two azido ligands are *anti* and the third azide is *gauche* (see Figure 11 and Table 5). Our results are in reasonably good agreement with previous HF/6–31+G* and BLYP computations[19] for $As(N_3)_3$ and $Sb(N_3)_3$ and with the experimentally observed values (see above). The most significant difference

is the length of the terminal N–N bonds, which is overestimated in our calculations by about 0.05 Å.

Vibrational spectra: The infrared and Raman spectra of $As(N_3)_3$ and $Sb(N_3)_3$ are shown in Figures 12 and 13, respectively. Tables 6 and 7 summarize the computed and observed frequencies. The vibrational spectra of both compounds demonstrate the presence of covalently bonded azido ligands. The presence of more than one azido ligand results in in-phase and out-of-phase coupling, and the internal azido modes split into two components. For C_3 symmetry, the out-of-phase E modes are doubly degenerate and, in some cases, can be split due to a lifting of the degeneracy. The observation of extra bands in the 1350 to 1100 cm^{-1} region is attributed to Fermi resonance of ν_2 and ν_{10} with the appropriate combination bands or overtones.

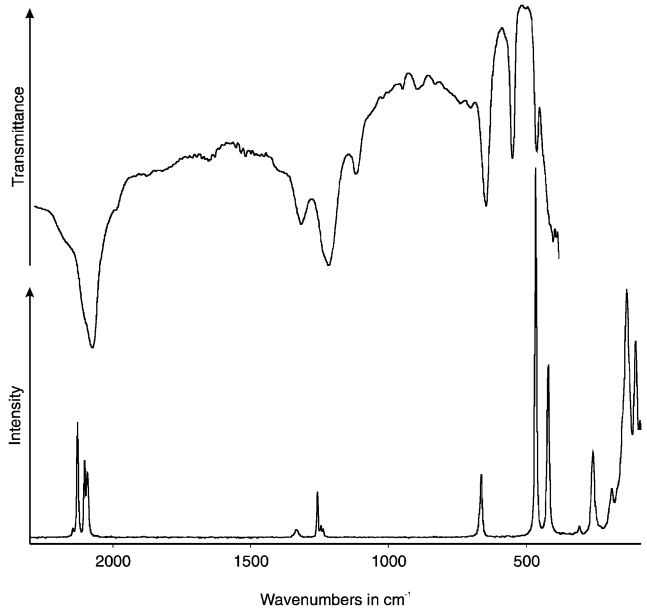

Figure 12. Infrared (upper trace) and Raman (lower trace) spectra of solid $As(N_3)_3$.

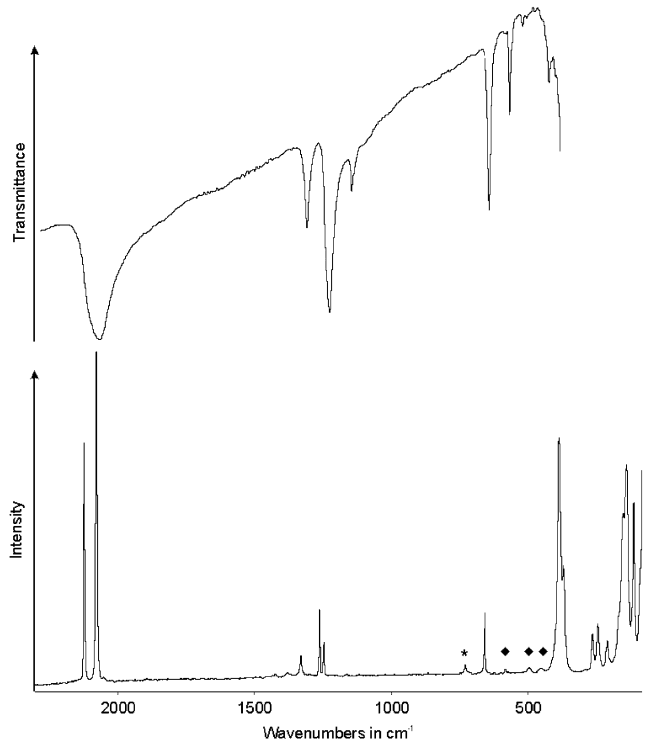

Figure 13. Infrared (upper trace) and Raman (lower trace) spectra of solid $Sb(N_3)_3$. The band marked by an asterisk is due to the FEP sample tube. Bands marked by ◆ are believed to be caused by a small amount of an unknown impurity.

For $As(N_3)_3$, the best fit between observed and computed frequencies is obtained for the C_3(**1**) isomer, in accord with the observed crystal structure. The fit between observed and calculated frequencies is good for both $As(N_3)_3$ and $Sb(N_3)_3$. As might be expected, the nitrogen bridging lowers the skeletal AsN_3 and SbN_3 stretching frequencies and increases those of the deformation modes. This effect is more pronounced for $Sb(N_3)_3$ because of the stronger bridging. The general agreement between the vibrational spectra of $As(N_3)_3$ and $Sb(N_3)_3$ is very good and supports our vibrational analysis. The only ambiguity is the observation of one weak Raman at 191 and 211 cm^{-1} in $As(N_3)_3$ and $Sb(N_3)_3$, respectively, which could not be accounted for in our assignments and were tentatively assigned to a stretching mode involving the nitrogen bridges.

Conclusion

The exact structures of the highly explosive $As(N_3)_3$ and $Sb(N_3)_3$ molecules have been determined for the first time. Both structures can be derived from an ideal C_3 symmetry with the azido ligands being bent away from the sterically active, free valence-electron pair of the central atom. Additional nitrogen bridging increases the coordination numbers of arsenic and antimony to seven. The basic motif for the nitrogen bridging are four-membered dimeric rings consisting of two As or Sb atoms and two α-nitrogen atoms from two azido ligands. For $As(N_3)_3$, only two of its three azido ligands participate in the association process, resulting in an infinite zigzag chain structure and destroying the perfect C_3 symmetry. For $Sb(N_3)_3$, however, all three azido ligands take part equally in the association and produce a highly symmetrical sheet structure, representing a case of perfect rhombohedral C_3 symmetry.

Experimental Section

Caution! *Arsenic and antimony azide compounds are potentially toxic and can decompose explosively under various conditions! They should be handled only on a scale of less than 2 mmol with appropriate safety precautions (safety shields, safety glasses, face shields, leather gloves, protective clothing, such as leather suits, and ear plugs). Teflon containers should be used, whenever possible, to avoid hazardous fragmentation. Ignoring safety precautions can lead to serious injuries.*

Materials and apparatus: All reactions were carried out in Teflon–FEP ampules that were closed by stainless steel valves. Volatile materials were handled in a stainless steel-Teflon-FEP or Pyrex glass vacuum line. All reaction vessels and the stainless steel line were passivated with ClF_3

Table 6. Comparison of observed and unscaled calculated MP2 vibrational frequencies [cm^{-1}] and intensities for C_3(**1**) $As(N_3)_3$.

Mode		Approx. mode description in point group C_3	Observed[a,g] IR	Raman	Calculated[b] (IR) [Raman]
A	ν_1	$\nu_{as}N_3$ in phase	2121 (vs)	2128 [3.1]	2255 (506.9) [6.7]
	ν_2	ν_sN_3 in phase	1251 (s,sh)[e]	1257 [1.2][e]	1293 (122.8) [22.1]
	ν_3	δN_3 in phase, in plane		663 [1.7]	681 (0.7) [16.6]
	ν_4	δN_3 in phase, out of plane			532 (0.2) [0.8]
	ν_5	ν_sAsN_3	480 (m)	465 [10.0]	507 (27.3) [23.4]
	ν_6	δAsN_3 in phase	[c]	307 [0.3]	325 (35.5) [0.4]
	ν_7	δAs-N-N in phase	[c]	102 [2.7]	94 (0.2) [1.0]
	ν_8	τ in-phase	[c]	[d]	57.4 (0.0) [8.6]
E	ν_9	$\nu_{as}N_3$ out of phase	2092 (vs)	2103 [2.1][e] 2093 [1.8][e]	2215 (298.3) [6.1]
	ν_{10}	ν_sN_3 out of phase	1231 (s)	1244 [0.3][e,f] 1237 [0.2][e,f]	1280 (92.8) [6.8]
	ν_{11}	δN_3 out of phase, in plane	664 (m)		673 (25.3) [2.4]
	ν_{12}	δN_3 out of phase, out of plane	568 (m)		532 (10.1) [0.7]
	ν_{13}	$\nu_{as}AsN_3$	420 (s)	419 [4.6]	459 (83.5) [4.7]
	ν_{14}	δAsN_3 out of phase	[c]	257 [2.3]	243 (8.8) [1.4]
	ν_{15}	δAs-N-N out of phase	[c]	135 [5]	113 (0.4) [5.9]
	ν_{16}	τ out of phase	[c]	[d]	44 (0.0) [4.4]

[a] Relative IR and Raman intensities given in parentheses and square brackets, respectively. [b] IR intensities given in km mol^{-1} and Raman intensities given in $Å^4 amu^{-1}$. [c] Not observed, IR spectrum recorded only between 4000 and 400 cm^{-1}. [d] Not observed, Raman spectrum recorded only between 4000 and 80 cm^{-1}. [e] Splittings caused by deviation from C_3 symmetry, resulting in lifting of the degeneracy. [f] These modes show the following Fermi resonance splittings: IR: 1337 cm^{-1} (m) ($\nu_3 + \nu_{11}$) (E); 1133 cm^{-1} (mw) ($\nu_5 + \nu_{11}$) (E); Raman: 1334 cm^{-1} [0.2] ($2\nu_3$ or $2\nu_{11}$) (A). [g] In addition to the listed bands, a Raman band at 191 cm^{-1} [1] was observed which was not assigned. It might represent a nitrogen-bridge stretching mode.

Table 7. Comparison of observed and unscaled calculated MP2 vibrational frequencies [cm^{-1}] and intensities for $Sb(N_3)_3$.

Mode		Approx. mode description in point group C_3	Observed[a] IR	Raman	Calculated[b] (IR) [Raman]
A	ν_1	$\nu_{as}N_3$ in phase	2121 (s,sh)	2123 [7.4]	2183 (631.9) [8.3]
	ν_2	ν_sN_3 in phase	1243 (vs)[d]	1263 [2.2] [d]	1243 (114.7) [37.8]
	ν_3	δN_3 in phase, in plane		660 [2.4]	653 (0.0) [20.7]
	ν_4	δN_3 in phase, out of plane			585 (0.2) [0.5]
	ν_5	ν_sSbN_3	[c]	386 [7.5]	456 (16.0) [39.9]
	ν_6	δSbN_3 in phase	[c]	289 [0.1]	258 (35.6) [0.8]
	ν_7	δSb-N-N in phase	[c]	115 [4]	91 (0.2) [1.4]
	ν_8	τ in-phase	[c]	[f]	78 (0.1) [7.5]
E	ν_9	$\nu_{as}N_3$ out of phase	2085 (vs)	2079 [10.0]	2140 (252.0) [14.5]
	ν_{10}	ν_sN_3 out of phase	1243 (vs) [d]	1248 [1.2] [d]	1231 (59.1) [5.7]
	ν_{11}	δN_3 out of phase, in plane	659 (s)		643 (7.0) [1.9]
	ν_{12}	δN_3 out of phase, out of plane	583 (m)		567 (3.3) [0.5]
	ν_{13}	$\nu_{as}SbN_3$	[c]	370 [3]	414 (70.7) [5.4]
	ν_{14}	δSbN_3 out of phase	[c]	264 [1.8] [e] 247 [1.5]	199 (9.0) [1.1]
	ν_{15}	δSb-N-N out of phase	[c]	153 [4][e] 141[6.0]	109 (0.2) [7.0]
	ν_{16}	τ out of phase	[c]	[f]	56 (0.1) [4.2]

[a] Relative IR and Raman intensities given in parentheses and brackets, respectively.[b] IR intensities given in km mol^{-1} and Raman intensities given in $Å^4 amu^{-1}$. [c] Not observed, IR spectrum was recorded only between 4000 and 400 cm^{-1}. [d] These modes show the following Fermi resonance splittings: IR, 1326 cm^{-1} (m), ($\nu_3 + \nu_{11}$) (E); 1162 cm^{-1} (mw), ($\nu_5 + \nu_{11}$) (E); Raman: 1331 cm^{-1} [1.2], ($2\nu_3$ or $2\nu_{11}$) (A). [e] Splitting due to lifting of the degeneracy. In the low-frequency region, the following additional bands were observed and tentatively assigned: IR: 442 cm^{-1} (mw) νSbN_3; RA: 211 cm^{-1} [0.9], corresponding to the 191 cm^{-1} [1] band in $As(N_3)_3$. These Raman bands might represent stretching modes of the nitrogen bridges. [f] Not observed, Raman spectrum recorded only between 4000 and 80 cm^{-1}.

prior to use. Nonvolatile materials were handled in the dry argon atmosphere of a glove box.

Infrared spectra were recorded in the range 4000–400 cm^{-1} on a Midac FT-IR model 1720 at a resolution of 1 cm^{-1}. Spectra of solids were obtained by using dry powders pressed between AgCl windows in an Econo press (Barnes Engineering Co.). Raman spectra were recorded in the range 4000–80 cm^{-1} on a Bruker Equinox 55 FT-RA spectrophotometer using a Nd:YAG laser at 1064 nm with power levels of 100 mw or less. Pyrex melting point tubes that were baked out at 300 °C for 48 h at 10 mTorr vacuum or Teflon–FEP tubes with stainless steel valves that were passivated with ClF_3 were used as sample containers.

^{14}N NMR spectra were recorded at 36.13 MHz on a Bruker AMX 500 spectrometer in CH_2Cl_2 in sealed standard glass tubes. Neat CH_3NO ($\delta =$ 0.00 ppm) was used as external reference for ^{14}N.

The $(CH_3)_3SiN_3$ (Aldrich) and AsF_3 (Ozark) were purified by fractional condensation prior to use. The SbF_3 (Alfa Aesar) was purified by sublimation. The SO_2 (Aldrich) was condensed into a bulb and dried over CaH_2.

Preparation of $As(N_3)_3$: On the stainless steel vacuum line, AsF_3 (0.23 mmol) was condensed at −196 °C into a Teflon–FEP ampule. The ampule was then attached to a glass vacuum line and after evacuation, SO_2 (3.3 mmol) was condensed in at −196 °C. The mixture was allowed to warm to ambient temperature. After all the AsF_3 had dissolved, the ampule was cooled back again to −196 °C, and $(CH_3)_3SiN_3$ (0.885 mmol) was added. The ampule was kept at −40 °C for 30 min and then slowly warmed to room temperature over a period of 4 h, resulting in a colorless solution. The volatile components were pumped off, leaving behind a white solid (0.045 g, weight calculated for 0.23 mmol $As(N_3)_3 = 0.046$ g). Further pumping at ambient temperature led to the sublimation of the crude product resulting in the formation of crystalline material on the walls of the reaction vessel. Inspection of the volatile material trapped at −196 °C by gas-FTIR spectroscopy showed SO_2 and $(CH_3)_3SiF$[20,21] as the only reaction by-products. The crystalline solid was identified as $As(N_3)_3$ by vibrational and NMR spectroscopy and its crystal structure.

Preparation of $Sb(N_3)_3$: A sample of SbF_3 (0.47 mmol) was loaded in the dry box into a Teflon–FEP ampule, followed by the addition of SO_2 (5.8 mmol) in vacuo at −196 °C. The

mixture was warmed to room temperature to suspend the SbF_5 in the SO_2, cooled back again to −196 °C, and $(CH_3)_3SiN_3$ (2.16 mmol) was condensed in. The ampule was kept at −40 °C for 30 min and then slowly warmed to ambient temperature over a period of 4 h. Volatile components were pumped off and collected at −196 °C, leaving behind a white solid residue (0.120 g, weight calculated for 0.47 mmol of $Sb(N_3)_3$ = 0.116 g). The only volatile byproduct, identified by gas-FTIR spectroscopy, was $(CH_3)_3SiF$. The crude $Sb(N_3)_3$ was vacuum sublimed in a sealed glass tube at 100–110 °C. The obtained colorless crystals were characterized by vibrational and NMR spectroscopy and their crystal structure.

Crystal structure determinations: The single-crystal X-ray diffraction data were collected on a Bruker three-circle platform diffractometer, equipped with a SMART CCD (charge coupled device) detector, with the χ axis fixed at 54.74° and with $Mo_{K\alpha}$ radiation ($\lambda = 0.71073$ Å) from a fine-focus tube. An LT-3 apparatus was employed for the low-temperature data collection by using controlled liquid nitrogen boil off. A few well-formed single crystals, prepared by careful sublimation of the amorphous solid, were selected in a glove box, by using a CCD camera microscope. The selected crystals were immersed in PFPE (perfluoropolyether) oil, contained in the cavity of a culture slide. A Cryoloop was used for picking a crystal and mounting it on a magnetic goniometer head. Cell constants were determined from ninety 10 s frames. A complete hemisphere of data was scanned on omega (0.3°) with a run time of 30 s per frame at a detector resolution of 512 × 512 pixels using the SMART software.[22] A total of 1271 frames was collected in three sets and a final set of 50 frames, identical to the first 50 frames, was also collected to determine any crystal decay. The frames were then processed on a PC running on Windows NT software. The SAINT software[23] was used to obtain the *hkl* file corrected for Lp/decay. The absorption correction was performed by using the SADABS program.[24] For $As(N_3)_3$, the intensity statistics, that is, E^2-1 values, indicated a centrosymmetric space group. Furthermore, the absence of $0k0$ (k = odd) and $h0l$ reflections ($h+L$ = odd) showed the presence of a 2_1 screw axis and a *c*-glide plane parallel and perpendicular to the *b* axis, respectively. The space group was thus unambiguously assigned as $P2_1/c$. For $Sb(N_3)_3$, the reciprocal lattice was initially indexed as a hexagonal cell with cell constants of $a = 7.2046$ (10), $c = 19.439(4)$ Å, $V = 873.8(2)$ Å^3, and $Z = 6$. An alternate setting with a smaller rhombohedral cell was obtained by using the transformation matrix $\{^2/_3, {}^1/_3, {}^1/_3, {}^{-1}/_3, {}^1/_3, {}^1/_3, {}^{-1}/_3, {}^{-2}/_3, {}^1/_3\}$ with cell constants of $a = 7.6998(9)$, $\alpha = 55.787(17)°$, $V = 291.26(6)$ Å^3, and $Z = 2$. The structures were solved by the Patterson method by using the SHELX-90 program[25] and refined by the least-squares method on F^2, SHELXL-97,[26] incorporated in the SHELXTL Suite 5.10 for Windows NT.[27] All atoms were refined anisotropically. For the anisotropic displacement parameters, the U_{eq} is defined as one third of the trace of the orthogonalized U_{ij} tensor. For generating the difference electron density contours the $F_o - F_c$ was calculated by using the "EDEN" feature of the SHELXTL program.[27] The difference $F(000)$ value of 2 was used to compute the lone pair contour. Further details of the crystal investigations can be obtained from the Fachinformationszentrum Karlsruhe, 76344 Eggenstein-Leopoldshafen, Germany (Fax: (+49) 7247-808-666; E-mail: crysdata@fiz-karlsruhe.de) on quoting the depository numbers CSD-413359 and CSD-413360 for $Sb(N_3)_3$ and $As(N_3)_3$, respectively.

Computational methods: Optimizations of all structures were performed by using second-order perturbation theory.[17,18] . For $As(N_3)_3$, the Binning and Curtis double-zeta valence basis set,[28] augmented with a d-polarization function[29] was used for arsenic and the 6–31G(d) basis set[30,31] for nitrogen. For $Sb(N_3)_3$, the Stevens, Basch, and Krauss effective core potentials and the corresponding valence-only basis sets were used.[32] The SBK valence basis set for nitrogen was augmented with a d-polarization function[31] and a diffuse s+p shell,[33] whereas only a d-polarization function[34] was added to the antimony basis set. Hessians (energy second derivatives) were calculated for the final equilibrium structures to determine if they are minima (positive definite hessian) or transition states (one negative eigenvalue). All calculations were performed with the electronic structure code GAMESS.[35]

Acknowledgement

We are grateful to the National Science Foundation, the Air Force Office of Scientific Research and Defense Advance Research Projects Agency for financial support. R.H. is grateful to the Deutsche Forschungsgemeinschaft for a stipend. A grant of computer time by the Department of Defense High-Performance Computing Modernization Program at the Aeronautical Systems Center (Wright-Patterson AFB, OH) and Army High Performance Computing Research Center (Minneapolis, MN) is gratefully acknowledged.

[1] T. M. Klapötke, P. Geissler, *J. Chem. Soc. Dalton Trans.* **1995**, 3365.
[2] T. M. Klapötke, A. Schulz, J. McNamara, *J. Chem. Soc. Dalton Trans.* **1996**, 2985.
[3] K. Karaghiosoff, T. M. Klapötke, B. Krumm, H. Nöth, T. Schütt, M. Suter, *Inorg. Chem.* **2002**, *41*, 170.
[4] For recent reviews, see W. Fraenk, T. M. Klapötke, in *Inorganic Chemistry Highlights* (Eds.: G. Meyer, D. Naumann, L. Wesemann), Wiley-VCH, Weinheim, **2002**; T. M. Klapötke, *Chem. Ber.* **1997**, *130*, 443.
[5] a) U. Mueller, H. Baernighausen, *Acta Crystallogr. Sect B* **1970**, *26*, 1671; b) W. Kolitsch, U. Mueller, *Z. Anorg. Allg. Chem.* **1974**, *410*, 21; c) M. A. Petrie, J. A. Sheehy, J. A. Boatz, G. Rasul, G. K. S. Prakash, G. A. Olah, K. O. Christe, *J. Am. Chem. Soc.* **1997**, *119*, 8802.
[6] S. F. Boys, *Quantum Science of Atoms, Molecules, and Solids* (Ed.: P. O. Lowdin), Academic Press, NY, **1966**, pp. 253–262.
[7] R. F. W. Bader, *Atoms in Molecules: A Quantum Theory*, Clarendon, Oxford, **1990**.
[8] T. M. Klapötke, H. Nöth, T. Schütt, M. Warchold, *Z. Anorg. Allg. Chem.* **2001**, *627*, 81.
[9] R. Haiges, J. A. Boatz, M. Gerken, S. Schneider, T. Schroer, K. O. Christe, *Angew. Chem.* **2003**, *115*, 6027; *Angew. Chem. Int. Ed.* **2003**, *42*, 5847.
[10] B. Neumüller, F. Schmock, S. Schlecht, K. Dehnicke, *Z. Anorg. Allg. Chem.* **2000**, *626*, 1972.
[11] M. Atam, U. Mueller, *J. Organomet. Chem.* **1974**, *71*, 435.
[12] S. Schroeder, W. Preetz, *Z. Anorg. Allg. Chem.* **2001**, *627*, 390.
[13] M. Herberhold, A.-M. Dietel, W. Milius, *Z. Anorg. Allg. Chem.* **1999**, *625*, 1885.
[14] M. Herberhold, A. Goller, W. Milius, *Z. Anorg. Allg. Chem.* **2001**, *627*, 891.
[15] J. P. Johnson, G. K. MacLean, J. Passmore, P. S. White, *Can. J. Chem.* **1989**, *67*, 1687.
[16] P. Geissler, T. M. Klapötke, H.-J. Kroth, *Spectrochim. Acta* **1995**, *51A*, 1075.
[17] a) C. Moller, M. S. Plesset, *Phys. Rev.* **1934**, *46*, 618b) J. A. Pople, J. S. Binkley, R. Seeger, *Int. J. Quantum Chem. S10*, **1976**, 1; c) M. J. Frisch, M. Head-Gordon, J. A. Pople, *Chem. Phys. Lett.* **1990**, *166*, 275.
[18] R. J. Bartlett, D. M. Silver, *Int. J. Quantum Chem. Symp.* **1975**, *9*, 1927.
[19] T. M. Klapötke, A. Schulz, *Main Group Met. Chem.* **1997**, *20*, 325.
[20] K. Licht, P. Koehler, H. Kriegsmann, *Z. Anorg. Allg. Chem.* **1975**, *415*, 31.
[21] H. Bürger, *Spectrochim. Acta* **1968**, *24A*, 2015.
[22] SMART V 4.045 Software for the CCD Detector System, Bruker AXS, Madison, WI, **1999**.
[23] SAINT V 4.035 Software for the CCD Detector System, Bruker AXS, Madison, WI, **1999**.
[24] SADABS Program for absorption correction for area detectors, Version 2.01, Bruker AXS, Madison, WI, **2000**.
[25] G. M. Sheldrick, SHELXS-90, Program for the Solution of Crystal Structure, University of Göttingen, Germany, **1990**.
[26] G. M. Sheldrick, SHELXL-97, Program for the Refinement of Crystal Structure, University of Göttingen, Germany, **1997**.
[27] SHELXTL 5.10 for Windows NT, Program library for Structure Solution and Molecular Graphics, Bruker AXS, Madison, WI, **1997**.
[28] R. C. Binning, Jr., L. A. Curtiss, *J. Comput. Chem.* **1990**, *11*, 1206.
[29] A d-function polarization exponent of 0.293 was used.

[30] W. J. Hehre, R. Ditchfield, J. A. Pople, *J. Chem. Phys.* **1972**, *56*, 2257.
[31] The exponent of the d-polarization function on N is 0.8; see P. C. Hariharan, J. A. Pople, *Theor. Chim. Acta* **1973**, *28*, 213.
[32] W. J. Stevens, H. Basch, M. Krauss, *J. Chem. Phys.* **1984**, *81*, 6026.
[33] The exponent of the diffuse s+p shell is 0.0639; see T. Clark, J. Chandrasekhar, G. W. Spitznagel, P. von R. Schleyer, *J. Comput. Chem.* **1983**, *4*, 294.
[34] The exponent of the d polarization function on Sb is 0.211; seeS. Huzinaga, J. Andzelm, M. Klobukowski, E. Radzio-Andzelm, Y. Sakai, H. Tatewaki, *Gaussian Basis Sets for Molecular Calculations*, Elsevier, Amsterdam, **1984**.
[35] M. W. Schmidt, K. K. Baldridge, J. A. Boatz, S. T. Elbert, M. S. Gordon, J. H. Jensen, S. Koseki, N. Matsunaga, K. A. Nguyen, S. Su, T. L. Windus, *J. Comput. Chem.* **1993**, *14*, 1347.

Received: August 27, 2003 [F5482]

